distance from the GC in much less than the solar Kelvin time, they may not have returned to the main sequence if they were strongly perturbed by the tidal field of the black hole. A strong tidal perturbation would also cause them to be in rapid rotation (W. Benz and J. G. Hills, in preparation).

All active galactic nuclei (AGNs) eject hyper-velocity stars which become intergalactic tramps. The expansion of the universe gradually slows them down with respect to the Hubble flow until they are captured by galaxies. Hyper-velocity stars from AGNs may constitute a minor impurity of metal-rich stars in the Galactic halo.

If hyper-velocity stars are not found, it may still be possible to retain the hypothesis of a massive GC black hole by arguing that my estimate of the binary frequency in the GC is too optimistic, that most GC stars are less massive, so fainter, than the Sun, or that exchange collisions between binaries and stellar remnants (white dwarfs, neutron stars, and small black holes) have allowed these hard-to-detect objects to replace so many main-sequence stars in GC binaries that few main-sequence stars are left in them[10]. But the detection of even one hyper-velocity star coming from the GC would be nearly definitive proof of its having a massive black hole.

After an exchagne collision with a $10^6\ M_\odot$ black hole, the semi-major axis of the binary is typically 50 AU for $a_0 = 0.01$ AU and 500 AU for $a_0 = 0.1$ AU. The r.m.s. orbital velocity, $V_{\rm orbital}$, of the star about the black hole is nearly the same as the ejection velocity, V_∞, of its former companion, or about 4,000 and 1,400 km s^{-1} respectively for these two binaries.

The velocity of an unbound star which collides with one of these bound stars exceeds the local parabolic speed which is, on average, about $\sqrt{2}\,V_{\rm orbital}$, so the two stars collide at an average speed of about $\sqrt{3}\,V_{\rm orbital} = 6{,}900$ and 2,400 km s^{-1} for the two cases. The minimum collision velocity required to break up two equally massive main-sequence stars is only about 2.3 times the escape velocity from their surface, or about 1,400 km s^{-1} (ref. 11). Most of the debris from the colliding stars should remain bound to the black hole and eventually be accreted by it.

The orbit of the bound star around the black hole is very eccentric, but tidal energy dissipation at pericentre may be able to circularize it before the star is destroyed in a stellar collision. Because of angular momentum conservation, the final semi-major axis of the circularized orbit will be about $a_f = 2R_{\rm min}$. Many tidal stars can accumulate in these close orbits because the high velocities in them make them very 'stiff', so it is very difficult for stars in other bound orbits to perturb them gravitationally.

The tidal energy dissipated in circularizing the orbits of stars captured in an exchange collision with a $10^6\ M_\odot$ black hole is ~0.1–1% of their rest-mass energy, or 10^{51-52} erg for a $1\ M_\odot$ star. (Comparable energy is released in one final supernova-class cataclysm when a tidal star in a nearly circularized orbit collides with an unbound star.) The radius of the captured tidal star increases, eventually following its Hayashi track, until its luminosity matches its rate of tidal energy dissipation. If each tidal star emits 10^{51} erg before its destruction in a collision and one is captured every 10^4 yr, the total integrated luminosity of the tidal stars orbiting the GC black hole is $\sim 10^6\ L_\odot$. The maximum luminosity of an individual star is its Eddington value, so at least 30 solar-mass stars are needed to produce the integrated luminosity. The integrated spectrum of these stars should mimic that of a giant with its absorption lines washed out by the extreme differential Doppler motion resulting from the high orbital velocities (0.03–0.1 c), of the individual tidal giants. The GC black hole may have accumulated a large number of these low-mass tidal giants in orbits with semi-major axes, a_t, on the order of few times $R_{\rm min}$. It is tempting to identify a_t with radius of the GC radio source, ~10 AU. Stellar winds and Roche overflow from the tidal giants may terminate any accretion disk beyond a_t.

Stellar remnants such as neutron stars, small black holes, and white dwarfs do not suffer appreciable tidal dissipation, so they tend to remain in their original post-exchange orbits. The GC black hole can accumulate a large number of these stellar remnants in orbits with semi-major axies of 50–500 AU and orbital velocities of 1,000–4,000 km s^{-1}. They are 'meat grinders' which help provide fuel for their master, the central black hole, by tearing material from main-sequence stars and giants that pass near them.

Received 18 August; accepted 18 November 1987.

1. Oort, J. H. *A. Rev. Astr. Astrophy.* **15**, 295-362 (1977).
2. Hills, J. G. *Nature* **254**, 295-298 (1975).
3. Hills, J. G. *Mon. Nat. R. astr. Soc. Soc.* **182**, 517-536 (1978).
4. Hills, J. G. & Fullerton, L. W. *Astr. J.* **85**, 1281-1291 (1980).
5. Shampine, L. F. & Gordon, M. K. *Computer Solution of Ordinary Differential Equations: The Initial Value Problem* (Freeman, San Francisco, 1975).
6. Aarseth, S. J. & Hills, J. G. *Astr. Astrophy.* **21**, 255-263 (1972).
7. Heggie, D. C. *Mon. Nat. R. astr. Soc.* **173**, 729-788 (1975).
8. Hills, J. G. *Astr. J.* **80**, 809-825 (1975).
9. Sellgren, K., Hall, D. N. B., Kleinmann, S. G. & Scoville, N.Z. *Astrophys. J.* **317**, 881-891 (1987).
10. Hills, J. G. *Mon. Nat. R. astr. Soc.* **175**, 1p-4p (1976).
11. Benz, W. & Hills, J. G. *Astrophys. J.* **323**, 614-628 (1987).

Laboratory simulation of Jupiter's Great Red Spot

Joël Sommeria*, Steven D. Meyers & Harry L. Swinney

Center for Nonlinear Dynamics and the Department of Physics, The University of Texas, Austin, Texas 78712, USA

Isolated large stable vortices have long been observed in the jovian atmosphere and more recently on Saturn. The existence of such stable vortices in strongly turbulent planetary atmospheres is a challenging problem in fluid mechanics. In a numerical simulation Marcus[1] found that a single stable vortex developed for a wide variety of conditions in a turbulent shear flow in a rotating annulus. To test this we conducted an experiment on a rotating annulus filled with fluid pumped in the radial direction. The annulus rotates rigidly (there is no differential rotation), but the action of the Coriolis force on the radially pumped fluid produces a counter-rotating jet. Coherent vortices spontaneously form in this turbulent jet, and for a wide range of rotation and pumping rates the flow evolves until only one large vortex remains.

Figure 1 shows the annular tank used in the experiments. The tank is rotated rapidly to achieve an essentially geostrophic flow (a two-dimensional flow in which the Coriolis force is balanced by pressure gradients[2]). In such a flow the inertial force is small compared with the Coriolis force, that is, the Rossby number is small. In our system the Rossby number is ~0.1, as estimated from the ratio of the characteristic time for the inertial force (the turnover time for a vortex) to the characteristic time for the Coriolis force (the rotation period of the tank).

On Jupiter the Great Red Spot and other persistent coherent vortices lie in latitudinal zones of strong shear[3]. Marcus's numerical simulation indicates that in a quasi-geostrophic flow the existence of a strong shear can lead to the formation of a single persistent coherent vortex. In our experiment there is a strong shear on the outer edge of the counter-rotating jet (see Fig. 2).

Dissipation appears to play little role in the dynamics of the jovian atmosphere[4], and the simulation by Marcus was done for an inviscid fluid. Our experiment is unusual in that the dynamical timescales of interest are typically an order of magnitude shorter than the viscous timescale. For example, the Ekman spin-down time t_E is typically 20 s while the vortex turnover time is only 2 s. (Measurements of t_E agree well with the calculated value, $t_E = h_0/2(\Omega\nu)^{1/2}$, where ν is the kinematic viscosity, Ω is the angular velocity of the tank, and h_0 is the mean depth

* Permanent address: Madylam, ENSHMG, BP 95, 38402 St Martin D'Hères Cedex, France.

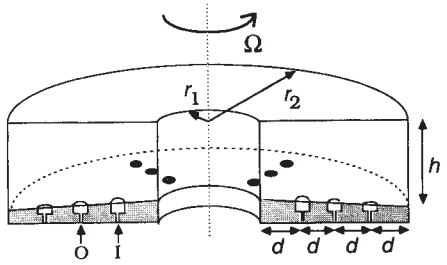

Fig. 1 The apparatus: $r_1 = 10.8$ cm, $r_2 = 43.2$ cm, $d = 8.1$ cm, $h(r_1) = 17.1$ cm and $h(r_2) = 20.3$ cm. The total flow rate F ranged from 15 to 370 cm^3 s^{-1}, and the rotation rate Ω ranged from 0 to 25 rad s^{-1}. A counter-rotating jet was produced by the action of the Coriolis force on the fluid (water) pumped into the tank through a ring of six inlets (I) at $r = 18.9$ cm, and from the tank through a ring of six outlets (O) at $r = 27.0$ cm (the ring of ports at $r = 35.1$ cm was not used). The effect of this forcing on the boundary layers was minimized by using 500 small holes (0.08-cm diameter) instead of a single hole at each inlet and outlet.

of the tank.) The weak dissipation is balanced on average by the pumping of the fluid. The Reynolds number for the bulk flow is large (typically 5×10^4), but the Reynolds number for the thin boundary layers is small enough so that these layers are laminar.

In a planetary atmosphere the Coriolis force varies with latitude (the beta effect). This is mimicked in our tank by a radially sloping bottom (slope $s = -0.1$). The transparent cover of the tank is flat. These considerations of geostrophic balance, Ekman damping and the beta effect lead to the following equations of motion for the vorticity, $\omega = (\nabla \times \mathbf{u})_z$, in our system[1,2]:

$$(\partial/\partial t + \mathbf{u} \cdot \nabla)(\omega + \beta r) = \zeta - \omega/t_E, \qquad \nabla \cdot \mathbf{u} = 0 \qquad (1)$$

where $\mathbf{u}$ is the velocity, $\zeta = 2\Omega w/h_0$ is the rate of vorticity production due to the forcing (with w the vertical velocity at an inlet or outlet), r is the radial coordinate, and $\beta = 2\Omega s/h_0$ is the coefficient of the beta effect. Both terms on the right-hand side of equation (1) are small; hence the potential vorticity of a fluid parcel, given here by $\omega + \beta r$ (see refs 1, 2 and 18) is to a first approximation conserved as it is advected. Also, the horizontal divergent flow due to the pumping is very small (~1%) compared with the nondivergent azimuthal flow generated by the strong Coriolis force.

Evidence for a strong counter-rotating jet is presented in Fig. 2, which shows profiles of the mean azimuthal velocity U, the vorticity $\omega_b = dU/dr + U/r$, and the shear $\sigma = dU/dr - U/r$. For small pumping rates the jet is confined between the inlets and outlets, while for large pumping rates the jet fills the annulus. Figure 2 is for a case of moderate pumping, where the jet, broadened by the turbulent mixing of vorticity, is wider than the separation between the inlets and outlets. Cyclonic vorticity (same sign as Ω) and anticyclonic vorticity (opposite sign) are produced at the same rate, but the shear in Fig. 2 is everywhere cyclonic, as in a single shear layer. (The anticyclonic vorticity on the inner side of the jet corresponds mostly to solid body rotation without shear.) The asymmetry between cyclonic and anticyclonic shear is a consequence of the jet curvature, and would disappear in the limit of small jet width (relative to the radius).

The dependence of the width $2L$ and maximum velocity U_0 of the jet on the pumping and rotation rates (F and Ω) can be estimated from a straightforward physical argument: the torque arising from the action of the Coriolis force on the radially pumped fluid, $\int 2\Omega\langle u_r\rangle(2\pi r^2 h_0)\, dr = 4\pi\Omega\langle u_r\rangle h_0 r_m^2 d$, is balanced by the torque arising from the dissipation in the boundary layers, $\int rU(r)(2\pi r h_0)\, dr/t_E = 2\pi h_0 r_m^2 U_0 L/t_E$, where r_m is the radial position of the jet, d is the separation between the sources and sinks, and $\langle u_r\rangle = F/2\pi r_m h_0$ is the radial velocity averaged in time and along a perimeter. Equating these torques yields $U_0 L = 2\Omega\langle u_r\rangle t_E d$. (The same result for $U_0 L$ can be obtained by multiplying equation (1) by r^2 and integrating over the annulus.)

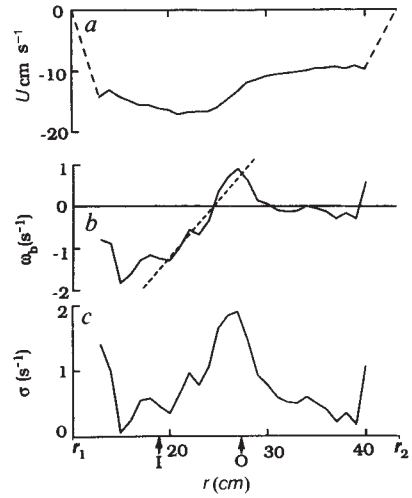

Fig. 2 *a*, The radial dependence of the azimuthal velocity $U(r)$, averaged in time and azimuth in a region far from any vortex. (The rotation rate was 25 rad s^{-1}; the total flow rate, 140 cm^3 s^{-1}). The velocity field was determined from analyses of photographs of particle streaks (see Fig. 3). *b*, The vorticity $\omega_b(r)$, determined from $U(r)$. The straight line is βr, corresponding to uniform potential vorticity (see text). *c*, The shear $\sigma(r)$, determined from $U(r)$. The spot is centred at the position of maximum shear. (The vertical arrows on the abscissa indicate the radial positions of the inlets (I) and outlets (O).)

Another relationship between L and U_0 can be obtained from the observation that the maximum slope of the vorticity, $d\omega_b/dr$, is approximately equal to β, as Fig. 2*b* shows. This result, which holds over a wide rage of Ω and F values, can be intepreted as a consequence of the mixing of potential vorticity by the turbulent flow. As $d\omega_b/dr \simeq U_0/L^2$, we have $U_0/L^2 = \beta$. Combining this expression for U_0/L^2 and the one for $U_0 L$ above we obtain

$$U_0 = c_1(F\Omega)^{2/3} \qquad (2)$$

$$L = c_2 F^{1/3}\Omega^{-1/6} \qquad (3)$$

where $c_1 = (sd^2/2\pi^2\nu h_0 r_m^2)^{1/3}$ and $c_2 = (dh_0/4\pi s r_m \nu^{1/2})^{1/3}$. Our measurements of the maximum velocity of the jet agree with equation (2) within 20% or better.

When the pumping rate is increased from low values with Ω held fixed, the jet develops (at $F \simeq 25$ cm^3 s^{-1}) an instability that results in the formation of a stable ring of five cyclonic vortices in the cyclonic shear on the outer side of the jet (see Fig. 3*a*). With a further increase in the pumping rate, a critical value is reached at which two vortices merge and a stable ring of four vortices forms (see Fig. 3*b*). Further increases in pumping rate lead to similar transitions to three and then to two stable vortices. At each of these steps the distance between the vortices increases more than the vortex size, and the position of the vortices fluctuates more and more as the flow becomes more turbulent with the increased forcing.

Finally, when the pumping rate is increased beyond ~100 cm^3 s^{-1}, we reach a regime with a single robust cyclonic vortex, see Fig. 3*e*. This regime persists to the highest flow rate achievable with our pump, 370 cm^3 s^{-1}. The single vortex moves with an average velocity equal to the local background flow and remains near the radial position of the sinks. Anticyclonic vortices also form in the turbulent flow, but they are always small and short-lived, disappearing in about one vortex turnover time.

The dynamics can be characterized in terms of two independent dimensionless parameters, chosen as

$$L^* = L/r_m \qquad (4)$$

$$T^* = t_E L/U_0 \qquad (5)$$

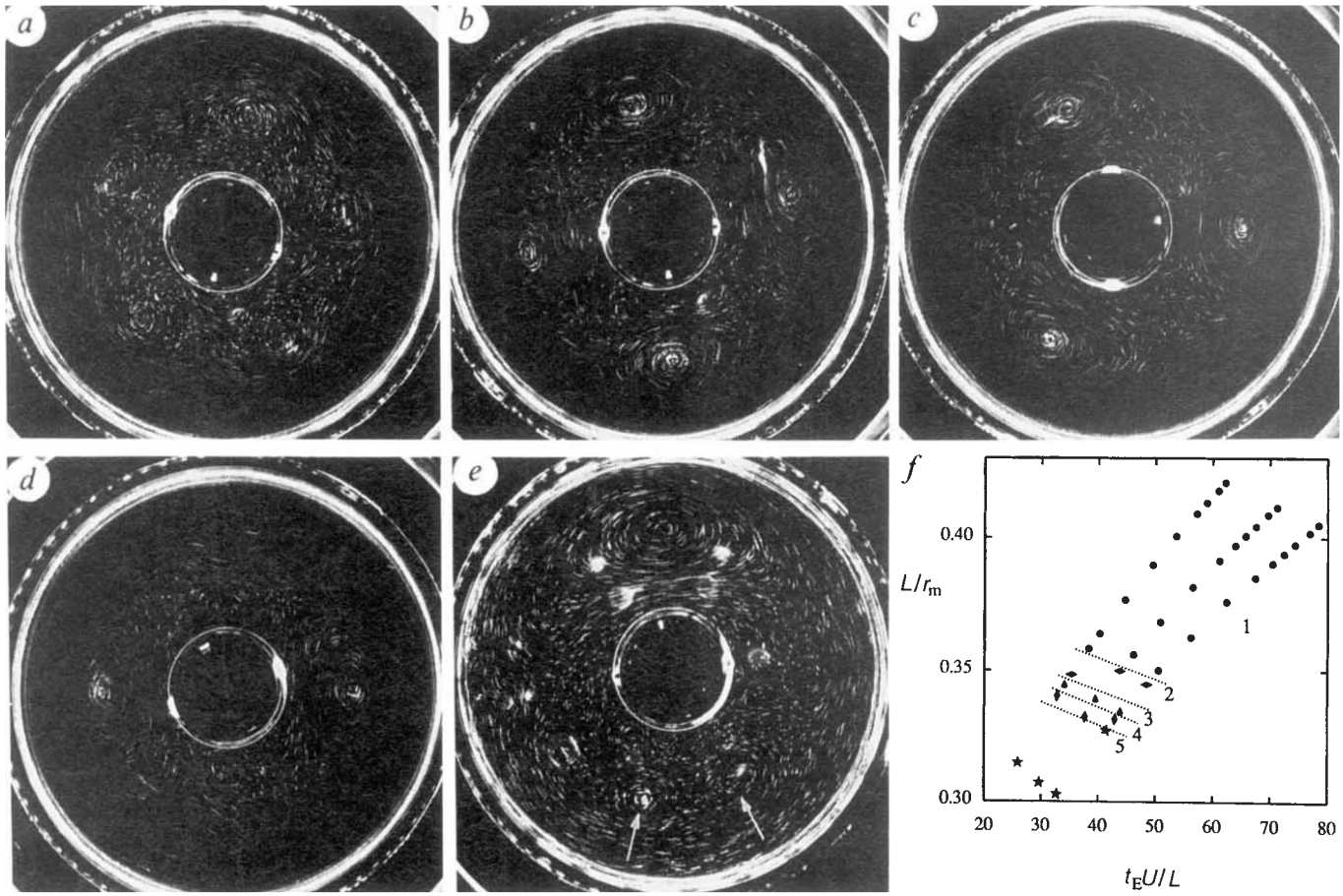

Fig. 3 Photographs of particle streaks for flows with different numbers n of persistent vortices: *a*, $n=5$; *b*, $n=4$; *c*, $n=3$; *d*, $n=2$; *e*, $n=1$. (The flow rates were, respectively, 25, 55, 66, 77, 185 $cm^3 s^{-1}$; tank rotation rates, 3, 3, 3, 3, 4 Hz; and photograph exposure times, 0.5, 0.5, 0.5, 0.5, 0.12 s.) The camera was rotating in the co-rotating frame of the average motion of the vortices, which in (*e*) was 0.8 rad s^{-1} slower than the rotation rate of the tank. Note that in (*e*), in addition to the main vortex, two smaller vortex pairs (indicated by arrows) can be seen to be in the process of merging. *f*, A regime diagram showing the dependence of the number of vortices as a function of the dimensionless jet size L^* and the ratio T^* of the Ekman friction time t_E to the vortex turnover time L/U (see text). Different symbols are used to distinguish regimes with different numbers of stable vortices, and dashed lines are shown to guide the eye in separating these regimes. The multiple vortex regimes are found only for small T^* where frictional effects are more important.

L^* is the dimensionless jet width and T^* is the ratio of the Ekman friction time to an eddy turnover time L/U_0. Substituting the expressions for L and U_0 from equations (2) and (3), we have

$$L^* = (c_2/r_m)F^{1/3}\Omega^{-1/6} \quad (6)$$

$$T^* = (h_0 c_1/2c_2\nu^{1/2})(F\Omega)^{1/3} \quad (7)$$

Figure 3*f* shows how the dynamics depends on these dimensionless parameters. The regime with a single persistent vortex is the dominant regime—multiple vortices are obtained only for small L^* and T^*.

When dye is injected inside a large vortex, it stays there for a long time with little indication of mixing with the outside fluid. When dye is injected outside a vortex, it is quickly mixed with the background turbulent flow, but does not penetrate the vortex, even after several minutes (see Fig. 4). The penetration of the dye is inhibited by a slow outward radial flow in the vortex, due to a recirculating current generated in the boundary layers. This circulation, called Ekman pumping[2], replaces the fluid inside the vortex in a typical time t_E. We can deduce from this that the turbulent diffusion across the vortex boundary into the vortex has a timescale t_E. The loss of dye from the vortex core occurs mainly during the merging of vortices.

In the regime with a single stable vortex, small cyclonic vortices are continually formed over the sinks, but they always merge with one another or with the dominant vortex. Figure 4 shows the vortex-merging process. The process is rapid, typically occurring in one vortex turnover time. In regimes with two or more stable vortices, mergings are not observed except when there is a transition between different regimes.

The dynamics leading to vortex mergers is easily understood. Because vortices move with the speed of the background flow, two vortices at different radii will move at different speeds, ultimately approaching one another. Then, if a secondary vortex is slightly downstream of the main vortex, it will be pushed outward by the flow of the main vortex and the background shear flow will carry the secondary vortex towards the main vortex. A similar process occurs when the secondary vortex is initially upstream.

When a secondary vortex is generated on the opposite side of the tank from the main vortex, but at the same radius, it can develop for a fairly long time, gaining in strength until it is comparable in size to the main vortex. However, this symmetrical arrangement is unstable—a fluctuation in the radial position of a vortex will result in the vortices approaching one another, and then they will quickly merge. When the forcing is increased, the fluctuations increase and the coexistence of vortices of comparable size becomes less and less frequent.

The main vortex grows by merger with smaller vortices until it fills the zone of strong shear. Then, in further mergers the excess vorticity feeds the background flow and often recoalesces

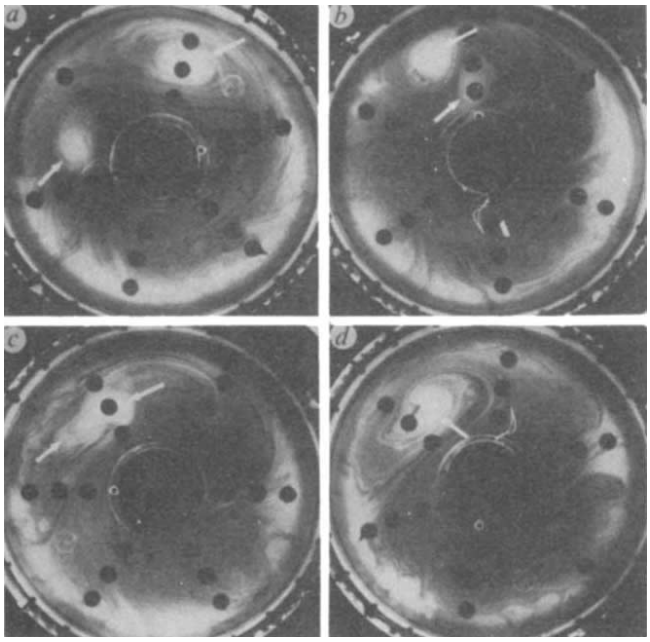

Fig. 4 The merging of two vortices (each indicated by an arrow) is illustrated in this sequence of photographs (taken at time intervals of 2 s) of the flow visualized with injected dye. The dye, injected outside of the vortices, does not reach the vortex cores. The 18 black dots are inlets and outlets in the bottom of the tank (see Fig. 1). The system is in the regime with a single stable vortex; the parameters are the same as in Fig. 3*e*.

into new small vortices; this can be observed in photographs of dye-containing vortices, which release part of the dye in the merging process.

The growth and merging of vortices observed in the experiments is very similar to that found in the numerical simulations of Marcus[1]—merging occurs in a time comparable with the vortex turnover time, and a vortex grows until it fills a shear zone. In the simulation the potential vorticity is uniform throughout the annulus, while in the experiment the region of uniform potential vorticity is limited to the azimuthal band in which the vortex is confined, and radiation of Rossby waves[2] is possible outside this band. In both the simulation and the experiment the vortices have about the same shape and magnitude relative to the background cyclonic shear flow, and cyclonic vortices are stable and anticyclonic vortices unstable in this flow. (In the simulation, anticyclonic vortices were found to be stable in an anticyclonic shear, but our experiment was not designed to produce a well-mixed anticyclonic shear; for example, if the direction of pumping in the experiment is reversed, a wavy coherent jet forms and there is little mixing.) Thus, although it is not possible to compare quantitatively the laboratory observations for a viscous fluid with the numerical simulation for an inviscid fluid, the qualitative properties of the vortices in the simulation are strikingly similar to those observed in the laboratory.

The vortices that we observe in the single vortex regime also have many properties in common with jovian vortices[3,5,6], including the following: vortices in the same latitudinal zone approach one another and quickly merge; they are usually located at a latitude of maximum shear; they have a vorticity with the same sign as the background shear (just as on Jupiter where anticyclonic spots occur in zones of anticyclonic shear and cyclonic barges occur in zones of cyclonic shear); they drift with the velocity of the background flow; the mean excess vorticity[1] of a spot is comparable to the background shear; and the spot length-to-width ratio is about two.

Our system, as a model of Jupiter, neglects the vertical structure of the jovian atmosphere, simplifying it to a single layer of uniform density and thickness. A refined model would include the interaction of the layer of strong eddy activity with layers above and below it. A measure of the vertical stratification is a horizontal length scale, called the Rossby radius of deformation[1], over which the surface of the fluid layers deform, intensifying or weakening lines of vorticity. The distribution of vorticity within a vortex thus depends on the Rossby radius, and in fact the maximum vorticity for jovian vortices is in an annular ring while our vortices have maximum vorticity at their centre. However, except for that difference, jovian vortex dynamics does not seem to be dramatically modified by the deformation—this view is supported by the observation that jovian spots range in size considerably ($\sim 10^3$-10^4 km), compared to the radius of deformation (estimated to be 1,000-5,000 km[1,6,7]).

In our experiment the Ekman pumping leads to a weak downwelling in the upper half of the centre of a vortex and a return flow on the outside of the vortex; similarly, there is an upwelling in the lower half of a vortex centre. Similar circulations have been observed in jovian vortices[7-9]. As in the experiment, such circulations could arise from a frictional mechanism, although the friction of upper atmospheric layers for jovian vortices would be different from that of the solid boundary in the experiment.

The forcing for our system is different from that on Jupiter, but our pumping could have an effect similar to the convective plumes penetrating into the jovian atmosphere from below. Direct observations of the flow and of weak temperature gradients in the jovian atmosphere indicate that the behaviour is governed largely by quasi-horizontal inertial effects[9]; therefore, the details of the forcing mechanism may not actually be important in determining the eddy patterns, even though forcing is essential for maintaining the energy and momentum of the flow.

Previous experiments have also been conducted on flows driven by sources and sinks in rotating tanks[10,11], but those experiments did not have a strong shear. We believe that the shear is the main ingredient for the formation of stable vortices, not only in our study but also in previous experiments aimed at modelling long-lived jovian vortices[12,13]. Two-dimensional shear layers have a strong and general tendency to develop robust vortices of the same sign as the shear, and in fact rings of steady vortices have been observed in previous studies of annular shear flows[12-15]. However, previous observations of single isolated vortices have been limited to narrow ranges of experimental parameters.

In an experiment by Antipov *et al.*[12] shear was produced by differential rotation of annular rings in the bottom of a parabolic-shaped rotating tank. The free upper surface deformed in response to the pressure field induced by the flow. Vorticity sheets, similar to those above our rings of sinks and sources, were generated at the boundaries between the rings and the tank bottom. A stable anticyclonic vortex was observed to form and was interpreted to correspond to the propagation of a Rossby soliton[16,17]. With cyclonic shear Antipov *et al.* obtained a ring of cyclonic vortices, similar to our observations for small pumping rates. They observed no merging of vortices, which is consistent with their interpretation of the observed vortex as a Rossby soliton but contrasts with our observations and those for Jupiter. The Antipov *et al.* system is similar to ours, but there are two differences: (1) the scale of forcing, as discussed below, and (2) the dissipation, which was larger in their 1-cm-thick layer (for which $T^* \simeq 5$) than in our experiment (where $25 < T^* < 80$).

In another experiment Read and Hide[13] obtained a stable anticyclonic vortex (paired with a weaker cyclonic vortex) in a rotating annulus that was heated internally and cooled on the vertical sidewalls. The vertical structure of the flow was found to be consistent with the structure proposed for Jupiter. However, a single anticyclonic vortex was observed only in a

narrow laminar regime close to the transition from axisymmetric to non-axisymmetric flow, far from the regime of geostrophic turbulence. In the experiments of both Hide and Read and Antipov *et al.* the forcing was axisymmetric, which contrasts with the localized forcing produced by our pumping through inlets and outlets. The small scale of our forcing could be significant because such forcing is generally a necessary condition for strong turbulence in a quasi-two-dimensional flow (energy transfers towards small scales are inhibited).

Our experiment demonstrates that for a wide range of conditions a permanent coherent vortex, like the long-lived coherent spots on Jupiter, can emerge spontaneously from a turbulent, incompressible, quasi-geostrophic flow. It is not necessary to invoke stratification or deformation of the fluid layer to explain the formation of a stable spot. The dynamical behaviour is dominated by two-dimensional inertia and the beta effect; frictional effects are secondary, as on Jupiter.

Our experiments and the simulation of Marcus[1] suggest that long-lived vortices should form in planetary zones of strong shear and uniform potential vorticity. Recent estimates[18] indicate that the potential vorticity is fairly uniform for the zonal flows that contain the Great Red Spot and the White Oval BC, but further measurements are needed for other latitudes where long-lived vortices are located.

We thank Philip Marcus for suggesting this experiment. This research is supported by the NSF Program in Fluid Mechanics and Hydraulics, the Office of Naval Research Nonlinear Dynamics Program, and the Exxon Education Foundation. J.S. is supported in part by the Centre National de la Recherche Scientifique.

Received 16 June, accepted 11 December (1987).

1. Marcus, P. S. *Nature* **331**, 693-696 (1988).
2. Pedlosky, J. *Geophysical Fluid Dynamics* (Springer, New York, 1979).
3. Beebe, R. F. & Hockey, T. A. *Icarus* **67**, 96-105 (1986).
4. MacLow, M. M. & Ingersoll, A. P. *Icarus* **65**, 353-369 (1986).
5. Mitchell, J. L., Beebe, R. F., Ingersoll, A. P. & Garneau, G. W. *J. geophys Res.* **86**, 8751-8757 (1981).
6. Williams, G. P. *Adv. Geophys.* **28A**, 381-427 (1985).
7. Ingersoll, A. P. & Cuong P. G. *J. atmos. Sci.* **38**, 2067-2076 (1981).
8. Hatzes, A., Wenkert, D. D., Ingersoll, A. P. & Danielson, G.E *J. geophys. Res.* **86**, 8754-8749 (1981).
9. Flasar, F. M. *Icarus* **65**, 280-303 (1986).
10. Colin de Verdier, A. *Geophys. Astrophys. Fluid Dyn.* **15**, 213-251 (1980).
11. McEwan, A. D., Thompson, R. O. R. Y. & Plumb, R. A. *J. Fluid Mech.* **9**, 655-672 (1980).
12. Antipov, S. V., Nezlin, M. V., Snezhkin, E. N. & Trubinikov, A. S. *Nature* **323**, 238-240 (1986).
13. Read, P. L. & Hide, R. *Nature* **308**, 45-48 (1984).
14. Hide, R. & Titman, C. W. *J. Fluid Mech.* **29**, 39-60 (1967).
15. Rabaud, M. & Couder, Y. *J. Fluid Mech.* **136**, 291-319 (1983).
16. Maxworthy, T. & Redekopp, L. G. *Icarus* **29**, 261-271 (1976).
17. Petviashvili, V. I. *Soviet Astr. Lett.* **9**, 137-138 (1983).
18. Dowling, T. E. & Ingersoll, A. P. *J. atmos. Sci.* **45** (1988).

Numerical simulation of Jupiter's Great Red Spot

Philip S. Marcus

Department of Mechanical Engineering, University of California at Berkeley, Berkeley, California 94720, USA

Jupiter's Great Red Spot is viewed as a vortex that arises naturally from the equations of motion of the jovian atmosphere. Here I solve numerically the equations governing fluid motion in a model of the jovian atmosphere for a variety of initial conditions. Large spots of vorticity form spontaneously in chaotic azimuthal flows and are stable if the vorticity of the spots has the same sign as the shear of the surrounding azimuthal flow. The Great Red Spot is compared with these solutions and a new prediction of its vertical structure is made.

Following Ingersoll and Cuong[1], I use a two-layer model in which the Great Red Spot lies in a shallow layer overlying a deep azimuthal flow. In this model the shallow upper layer does not influence the denser flow beneath it, but the deep azimuthal flow affects the upper layer by determining its vertical depth. The velocity $\mathbf{v}$ of the upper layer is approximated as two-dimensional (due to the rapid rotation of the planet) and is determined by potential vorticity ω_p conservation:

$$\left[\frac{\partial}{\partial t}+(\mathbf{v}\cdot\nabla)\right]\omega_p \equiv \frac{D\omega_p}{Dt}=0 \tag{1}$$

We use the quasi-geostrophic β-plane approximation[2] for ω_p of the upper layer:

$$\omega_p(r,\phi,t)=\omega(r,\phi,t)-\beta r-\frac{\psi(r,\phi,t)-\bar{\psi}(r)}{L_R^2} \tag{2}$$

where β is the gradient of the Coriolis force, ϕ is the longitude, r is the latitude of Jupiter multiplied by its radius, $L_R \equiv (\sqrt{gH\Delta\rho/\rho})/f$ is the Rossby deformation radius (a measure of the vertical stratification), f is twice Jupiter's angular velocity, $\Delta\rho$ is the difference in density between the lower and upper layers, and ρ, H, g, $\psi(r,\phi,t)$ and $\omega(r,\phi,t)\equiv\nabla^2\psi(r,\phi,t)$ are the density, mean vertical depth, gravitational acceleration, stream function and vorticity of the upper layer. The azimuthal velocity of the lower layer is given by the stream function $\bar{\psi}(r)$. The physics responsible for the deep flow (convection, latent heat release, radiation and differential heating, for example) occurs on timescales that are much longer[1,3] (10^8 s) than the dynamical or turn-around time of the spot ($\sim 10^6$ s). (In the five months between the fly-bys of Voyagers 1 and 2, there was no appreciable change in Jupiter's azimuthal zones[4].) Therefore we treat $\bar{\psi}(r)$ as a time-independent, but unknown, parameter that we vary to obtain different numerical solutions. Here, equations (1) and (2) are solved numerically with spectral methods[5] and with impermeable boundaries at $r=R_1$ and R_2. We use cylindrical, rather than the usual cartesian coordinates in equations (1) and (2) to allow a direct comparison with the cylindrical laboratory experiments of Sommeria *et al*[6].

I adopt the hypothesis that the jovian zone containing the Great Red Spot is an approximately axisymmetric, azimuthal flow with nearly uniform ω_p that contains isolated patches of non-uniformity (including the red spot). Although the hypothesis cannot be tested directly because $\bar{\psi}(r)$ and L_R are unknown, it is consistent with their known bounds[1]. The motivation for this hypothesis is that numerical simulations have shown that fluids that obey equation (1) and that are mixed by external stirring tend to produce flows with nearly uniform ω_p over much of their domains[7,8]. This evolution to homogeneous ω_p has also been observed in the laboratory[6]. Our numerical simulations of equations (1) and (2) in an annular geometry with no stirring also show that large regions with homogeneous ω_p form when the initial velocity is random but constrained so that its azimuthal average, $1/(2\pi)\int_0^{2\pi} v_\phi(r,\phi,t=0)\,d\phi$, is a linearly unstable solution of equation (1)[9]. (All axisymmetric, azimuthal flows are exact solutions of equation (1).)

Typically, the nearly axisymmetric, azimuthal flows with uniform ω_p produced in our simulations and in the experiments of Sommeria *et al.* contain a few, small, isolated vortices where the value of ω_p differs substantially from that of the surrounding azimuthal flow. Because the evolution of a general class of initial flows into nearly uniform ω_p flows containing isolated vortices is discussed elsewhere[6,9], each numerical simulation presented here begins with an exactly axisymmetric, azimuthal, uniform ω_p flow superposed with a finite number of spots of vorticity. We define $\tilde{v}_\phi(r,t)$ as the velocity of the uniform ω_p component of the flow, $\sigma \equiv r\partial(\tilde{v}_\phi/r)/\partial r$ as its shear, and ω_e as the difference between the potential vorticity of a spot of vorticity and the ω_p of $\tilde{v}_\phi(r,t)$. Note that $\tilde{v}_\phi(r,t)$ is a neutrally stable solution of equation (1); it has no exponentially growing or decaying eigenmodes and cannot propagate Rossby waves[9].

First, I show that spots with ω_e the same sign as σ are stable and those with opposite sign are pushed to the radial boundaries